Improving the oceanic metric of the El Niño recharge oscillator model

Takeshi Izumo[1,2] and Maxime Colin[3,4,5]

[1] Institut de Recherche pour le Développement (IRD), EIO laboratory, Université de la Polynésie Française (UPF), Tahiti, French Polynesia

[2] formerly at IRD, Sorbonne Université - CNRS-IRD-MNHN, LOCEAN Laboratory, IPSL, Paris, France

[3]formerly at Climate Change Research Centre, University of New South Wales, Sydney, New South Wales, Australia

[4]Leibniz Centre for Tropical Marine Research, Bremen, Germany

[5]formerly at Laboratoire GEPASUD, University of French Polynesia, Tahiti, French Polynesia

Corresponding author: Takeshi Izumo (takeshi.izumo@ird.fr)

Submitted to GRL on February 22nd, 2022

Key Points:

- To improve the debated metric for the Recharge Oscillator, we develop an objective approach optimizing equations fit to observations.
- The recharge metric has to be based on oceanic heat content slow component independent from the fast zonal tilt mode.
- The optimal index is this independent component in the western and southwestern Pacific. It is better suited for operational diagnostics.

Abstract

The El Niño Southern Oscillation (ENSO) is the leading mode of interannual climate variability, with large socioeconomical and environmental impacts. ENSO main conceptual model, the Recharge Oscillator (RO), considers two independent modes: the fast zonal tilt mode in phase with central-eastern Pacific Temperature (T_e), and the slow recharge mode in phase quadrature. However, usual metrics do not orthogonally isolate the slow recharge mode, being correlated with T_e. Furthermore the optimal Oceanic Heat Content (OHC) region is currently debated. Here, through an objective approach to optimize RO equations fit to observations, we develop a new recharge index based on T_e-independent OHC_{ind} (T_e-variability regressed out). The optimal region is the western and southwestern Pacific (5°N-15°S,120°E-155°W): OHC_{ind_w+sw}. Southwestern Pacific OHC anomalies are caused by ENSO windstress and Ekman pumping meridional asymmetry. This index is more physically and statistically coherent, reconciling RO conceptual model with observations, and more relevant for ENSO operational forecasts.

Plain Language Summary

El Niño events and their counterparts La Niña events have important impacts globally. A key element for long-lead forecasts is the recharge state of the tropical Pacific Ocean, as captured in the Recharge Oscillator (RO) conceptual model. The RO considers two independent modes of oceanic variability, a fast variability and a slow recharge/discharge process. However, usual recharge indices mix these two modes of variability, and can thus lead to ambiguous operational diagnostics of the actual oceanic state. Furthermore, there is a geographical debate on the optimal recharge region. Here we develop a better index of the slow recharge process, independent of the fast mode. We use an objective approach optimizing the RO resemblance to observations to find the optimal index: the independent ocean heat content averaged over the western and southwestern tropical Pacific. We recommend the use of such a simple and unambiguous index for El Niño operational forecasts diagnostics.

1 Introduction

The El Niño Southern Oscillation (ENSO) is the leading mode of climate interannual variability, with large socioeconomic and environmental impacts (e.g. Neelin 1998, Wang and Picaut 2004, Clarke 2008, Timmerman et al. 2018, Jin et al. 2020 reviews). While ENSO predictability skill is now rather good at short leads, it has to be improved at longer leads (e.g. Barnston et al. 2012, 2019). One key element for long-lead seasonal forecasts is the recharge state of the tropical Pacific Oceanic Heat Content (OHC, equivalent to an increase of the thermocline depth *h* and of sea level anomaly SLA), as it brings long oceanic memory across ENSO phases. Its role is formalized in the Recharge Oscillator (RO) conceptual model of ENSO (e.g. Wyrtki 1985 ; Jin 1997a,b ; Meinen and McPhaden 2000 ; Clarke et al. 2007, Clarke 2010). E.g. during a La Niña, easterlies favor a slow accumulation of OHC in the western and equatorial Pacific. This recharge will progressively favor positive Sea Surface Temperature (SST) anomalies in the central-eastern equatorial Pacific (T_E) and thus El Niño onset through the Bjerkness positive feedback. The El Niño event will in turn lead to a discharge favoring a reversal to La Niña conditions, and so on. The RO can well explain ENSO cyclic nature (cf. section 3 for a detailed description of RO equations).

Yet there is a debate on which recharge metric to use. In the RO, the equatorial Pacific basin adjustment is separated into two independent modes. The fast mode associated to a zonal tilt of the thermocline is in phase with zonal equatorial wind stress τ_x and T_E. The slow recharge mode is in phase quadrature with the fast mode, i.e. with T_E. Several indices have been developed for this slow recharge mode that all bring predictability skill. Wyrtki (1985) and Jin (1997a,b) originally focussed on the western equatorial Pacific h_w. Jin's sketch, Meinen and McPhaden (2000), and Burgers et al. (2005) focussed on the mean equatorial h_{eq} (e.g. Warm Water Volume WWV; 5°N-5°S, 120°E-80°W), with $h_{eq} = h_{w+e}$, *i.e.* western (5°N-5°S, 120°E-155°W) + eastern (5°N-5°S, 155°W-80°W) boxes. h_{eq} (equivalently WWV) has become a widely-used ENSO recharge index. In theory, h_{eq} is independent from the fast tilt mode and thus from T_E within Jin (1997a,b) approximations. This independence/orthogonality property is essential, so that the h metric captures solely the slow recharge mode and does not mix it with the fast mode. But in the real world, h_{eq} is not independent. It is physically ambiguous, and thus potentially misleading: h_{eq} is dominated by a short-term Ekman convergence temporary *fast* "*increase*" in the *El Niño westerlies* case (thus not a true long-term recharge in the RO sense), two times larger than the long-term *slow discharge* expected from the RO theory (Izumo et al. 2018a; see also Neske and McGregor 2018). h_{eq} is hence firstly an index of the fast equatorial Kelvin wave rather than of the RO long-term recharge/discharge process. Thus h_{eq} is strongly positively correlated to τ_x and T_E. Hence, Izumo et al. (2018a) recommended the use of a western Pacific OHC index (in agreement with Ramesh and Murtugudde 2013; Boschat et al. 2013; Graham et al. 2015 ; Lai et al. 2015; Ballester et al. 2016a; Petrova et al. 2017; Jin et al. 2020). Yet, such western Pacific OHC index is also not independent from the fast zonal tilt mode, being partly negatively correlated to τ_x and T_E. h_w could thus also lead to ambiguous diagnostics of the actual oceanic state. E.g. a positive h_w anomaly does not necessarily represent a true recharge of the slow mode, but could also be due only to the fast tilt mode, for instance if we had just had a short-lived La Niña event instead of a long-lasting one.

Here we will hence develop an improved Pacific OHC index h_{ind} independent of T_E (i.e. independent of the fast tilt mode). And, without any a priori on the best h_{ind} region, we will develop an objective approach optimizing the skill of the RO differential equations fit to observations for the (T_E,h_{ind}) pair to find the best h_{ind} index, averaged over an extended optimal region objectively defined as the most skillful one.

2 Data and methods

Here we use classical monthly datasets: Optimum Interpolation SST OISSTv2 based on *in situ* observations and satellite measurements available from November 1981 onwards (Reynolds et al. 2002), CMAP1 precipitation (Xie and Arkin 1997), and windstress from ERA-I atmospheric reanalysis (Dee et al. 2011). We use the SLA as a proxy of OHC/WWV/thermocline depth anomalies, measured from satellites (CSIRO monthly dataset, 1992-2017, http://www.cmar.csiro.au/sealevel/sl_data_cmar.html). We subtract the 65°S-65°N global average at each time step to remove sea level rise global trend due to global warming.

For the ENSO index, T_E, we use the usual Niño3.4 region (170°W-120°W, 5°N-5°S), a reasonable compromise to capture central Pacific as well as eastern Pacific ENSO events (e.g.

Takahashi et al. 2011, Capotondi et al. 2015). We define T_E as Niño3.4 relative SST (RSST, i.e. SST minus its 20°N-20°S tropical mean), as recommended by Izumo et al. (2020) and Van Oldenborgh et al. (2021): atmospheric tropical deep convection interannual anomalies are rather related to RSST than to SST, notably in the presence of external forcing (see also Johnson and Kosaka 2016; Khodri et al. 2017; Izumo et al. 2018b; Williams and Patricola 2018, and Okumura 2019). Essentially, the deep convection threshold SST>~27-28°C (e.g. Gadgil et al. 1984) translates into RSST>~1°C, a threshold that remains valid in the global warming context (e.g. Johnson and Xie 2010). T_E is normalized (divided by its standard deviation; STD)

Here we use typical statistical methods. The monthly seasonal cycle computed over the full observation period is removed and intraseasonal variations are filtered out by a 4-month Hanning filter, so that periods lower than ~2-3 months are removed. Coefficients obtained from multivariate linear regressions are shown multiplied by the STD of their multiplying variable (h or h_{ind}, cf. section 3), so as to represent typical amplitudes (remember that STD(T_E) is already 1). 90% intervals of confidence are computed using the typical two-tailed Student t-test, with the effective degree of freedom computed using the formulae (30) of Bretherton et al. (1999).

3 Improving the Recharge Oscillator recharge index, h_{ind}

3.1 Towards new RO tendency equations for T_E and independent h_{ind}

The RO conceptual model of ENSO is based on the idea of recharge of western or equatorial Pacific OHC during La Niña and discharge during El Niño (Wyrtki 1985; Jin 1997a,b; see Jin et al. 2020 review for details on RO derivation). To derive its dT_E/dt tendency equation, some physically-reasonable assumptions are used. 1) τ_x is proportionnal to T_E, i.e. tropical deep convection and related τ_x respond quickly to T_E. 2) The fast oceanic response (i.e. quasi-instantaneous, timescales faster than ~2-3 months) to τ_x leads to a positive Bjerkness feedback term in the dT_E/dt equation (through both the zonal advective and thermocline feedbacks) that is proportional to τ_x and thus to T_E: $R_{BJ\_o}T_E$. 3) Atmospheric fluxes are approximated as a weak Newtonian damping proportional to T_E: $-r_{damp\_o}T_E$. 4) A deepening of the thermocline depth h related to a recharge in the equatorial Pacific favors positive T_E on time scales longer than 2-3 months: $F_1 h$ (see section 3.3 on mechanisms). Therefore:

$$\frac{dT_E}{dt} = R_o T_E + F_1 h \qquad (1)$$

the first term representing the net effect of Bjerkness positive feedback and Newtonian damping ($R_o = R_{BJ\_o} - r_{damp\_o}$) and the 2nd one the recharge/discharge influence on T_E (following Jin et al. 2020 notations).

Concerning dh/dt equation, in the RO, the slow recharge mode integrates temporally τ_x, thanks to the quasi-linear behavior of equatorial Pacific oceanic dynamics. E.g. negative T_E associated with easterly anomalies will progressively recharge the equatorial Pacific (see section 3.3 discussing mechanisms). This is formalized as a term $-F_{2\_o}T_E$ in the dh/dt equation:

$$\frac{dh}{dt} = -F_{2\_o} T_E - \varepsilon_o h \qquad (2)$$

the second term $-\varepsilon_o h$ being formally a Newtonian damping, expected to be weak.

I.e. the tendency equation for the vector $\begin{pmatrix} T_E \\ h \end{pmatrix}$ in matrix form is:

$$\frac{d\begin{pmatrix} T_E \\ h \end{pmatrix}}{dt} = \begin{pmatrix} R_o & F_1 \\ -F_{2_o} & -\varepsilon_o \end{pmatrix} \begin{pmatrix} T_E \\ h \end{pmatrix} \qquad (3)$$

This RO linear equation is simple, but there is a debate on the adequate *h* index to use. To resolve this debate objectively, an empirical way to find the best *h* is to have no *a priori* on the best region, and to search for the *h* region that statistically optimizes the correlation skill of this equation (3). In practice we do at each spatial point (x,y) two multivariate linear regressions:

$$\frac{dT_E(t)}{dt} = R_o(x,y)\, T_E(t) + F_1(x,y)\, h(x,y,t) + residual_T(\mathrm{x,y,t}) \qquad (4)$$

$$\frac{dh(x,y,t)}{dt} = -F_{2_o}(x,y)\, T_E(t) - \varepsilon_o(x,y)\, h(x,y,t) + residual_h(\mathrm{x,y,t}) \qquad (5)$$

The locations where the correlation skill for the $\begin{pmatrix} T_E(t) \\ h(x,y,t) \end{pmatrix}$ tendency equation is the highest should inform us of the best *h* region to represent the RO processes. This 2D skill for the $\begin{pmatrix} T_E \\ h \end{pmatrix}$ tendency equation in matrix form (3) is $r_{Te,h} = ((r_{Te}^2 + r_h^2)/2)^{1/2}$, where r_{Te} and r_h are the usual 1D correlation skills of the regressions of equations (4) and (5) separately.

Fig. 1a,c shows the dT_E/dt regression coefficients $R_o(x,y)$ and $F_1(x,y)$, multiplied by the STDs of T_E (=1) and *h*, so as to have their respective contributions to the regression. The best skill r_{Te} (Suppl. Fig. S1a) is found for $h(x,y,t)$ in the western equatorial (~5°N-5°S) and southwestern tropical (~5°S-15°S) Pacific, suggesting that the best region for averaging $h(x,y,t)$ could be the combination of these two regions. However, the contributions of the regression coefficients have a puzzling spatial distribution, with $R_o(x,y)$ varying strongly with e.g. a surprisingly strong negative sign for $R_o(x,y)$ in the equatorial central Pacific opposing a strong positive $F_1(x,y)$ contribution in the same region. This does not make much sense when looking for a good statistical decomposition.

The issue with regression (4) is that $T_E(t)$ and $h(x,y,t)$ are not statistically independent (i.e. not orthogonal), which makes it difficult to interpret physically the regression coefficients. We need to decompose $h(x,y,t)$ into its fast and slow components. A large component of *h* responds rapidly to τ_x and T_E. This fast response component of *h* is correlated to (i.e. linearly dependent of) T_E at timescales longer than ~2-3 months in the equatorial Pacific: Fig. 1i shows the downwelling pattern along the central to eastern equatorial Pacific (i.e. the fast temporary increase of OHC along the equatorial band, Izumo et al. 2018a, Neske and McGregor 2018) and

the zonal seesaw pattern with opposite anomalies in the western Pacific, i.e., the fast mode. So the pair of coordinates (T_E,h) is not the most relevant to describe the system evolution. We need to regress out from $h(x,y,t)$ this rapidly-responding component correlated to $T_E(t)$, so as to only focus on the slowly-responding independent component of h, hereafter h_{ind} (Fig. 3b of Izumo et al. 2018a). h_{ind} corresponds to the slow recharge mode related to the slower basin adjustment in disequilibrium with wind stress (e.g. Jin 1997ab, Alory and Delcroix 2002, Masuda et al. 2009, Clarke 2010, Fedorov 2010, Thual et al. 2013, Zhu et al. 2017, Izumo et al. 2018a). Thus, we can formally decompose h into a component linearly dependent of T_E and one independent of T_E :

$$h(x,y,t) = h_{fast\_mode(dependent,\ corr.\ to\ Te)} + h_{slow\_recharge\_mode(independent,\ uncorr.\ to\ Te)}$$

$$h(x,y,t) = K(x,y)\ T_E(t) + h_{ind}(x,y,t) \quad (6)$$

$K(x,y)$ being obtained from the linear regression of h onto T_E (Fig. 1i).

Equation (4) for dT_E/dt can then be rewritten as:

$$\frac{dT_E(t)}{dt} = R(x,y)\ T_E(t) + F_1(x,y)\ h_{ind}(x,y,t) + residual_T(\mathrm{x,y,t}) \qquad (7)$$

with $R = R_o + K\ F_1$

Fig. 1b,d shows the coefficients obtained from this multivariate regression (7) of dT_E/dt onto (T_E,h_{ind}) (the skill being also r_{Te}, as for (4); Suppl. Fig. 1a). R is uniformly negligible (~0.00±0.03 month^{-1}; Fig. 1b). F_1 varies spatially substantially, with the highest positive values in the western equatorial and southwest Pacific (Fig. 1d) corresponding to the highest skill r_{Te}.

For the h tendency equation formalizing the recharge/discharge process, using equation (5) based on (T_E,h) similarly leads to puzzling regression coefficients that are highly spatially-correlated and therefore superfluous (shown in Fig. 1e,g), again because of dependent h_{fast} component. This again suggests to use (T_E,h_{ind}) instead of (T_E,h) space. Equation (5) becomes:

$$\frac{dh_{ind}(x,y,t)}{dt} = -F_2(x,y)\ T_E(t) - \varepsilon(x,y)\ h_{ind}(x,y,t) + residual_{h_{ind}}(\mathrm{x,y,t}) \qquad (8)$$

With $F_2 = F_{2\_o} + \varepsilon_o\ K + K\ R_o + K^2 F_1$ and $\varepsilon = \varepsilon_o + K F_1$ (and $residual_{h_{ind}} = residual_h - K\ residual_T$). Fig. 1f,h shows these regression coefficients ε and F_2. The picture is clearer, more consistent with RO theory. ε is uniformly negligible, consistent with a weak damping (physically the damping due mainly to oceanic mixing, e.g. Fedorov 2010). F_2 is large in the western equatorial Pacific and even larger in the southwest Pacific. Equation (8) skill, r_{h_ind}, is also the largest in the western and southwestern Pacific (Suppl. Fig. 1b). Both dT_E/dt and dh_{ind}/dt regressions thus suggest that the best h_{ind} region should combine these two regions.

Here we explain the spatial patterns of Fig. 1's various panels. And why there are similarities among some of them. As ε is negligible, the temporal integral of equation (8) corresponds to the regression of h_{ind}(x,y,t) onto the temporal integral of T_E. So F_2 map shows us

how h_{ind}(x,y,t) would look like if ENSO windstress anomalies would blow for a long time, e.g. because of long-lasting La Niña conditions. The slow recharge would as expected be in the western Pacific, but interestingly also in the southwestern Pacific. This meridional asymmetry is caused by ENSO windstress asymmetry: e.g. westerlies shifted to the south during El Niño, plus a reversal to easterlies at ~15°S, related to an equatorward shift of the South Pacific Convergence Zone (SPCZ; Suppl. Fig. S2a; see also Alory and Delcroix 2002; Cibot et al. 2005). Associated asymmetric Ekman pumping (Suppl. Fig. S2b) forces locally downwelling (in the La Niña case) and thus slow off-equatorial downwelling Rossby waves progressively recharging the southwestern Pacific (*vice versa* for El Niño case). Ekman pumping asymmetry is mainly due to windstress curl (curl itself mostly due to $-d\tau_x/dy$; not shown), with some added asymmetry from beta τ_x term (Yokoi et al. 2008), large between ~7°S and 5°S (Suppl. Fig. S2b). Note that western boundary asymmetry would conversely favor a larger recharge in northwestern Pacific (Izumo et al. 2018a, their Fig. 5). Concerning F_1, F_1 physically represents the slow recharge mode influence on T_E (cf. section 3.3 on mechanisms). F_1 tends to have a similar pattern to F_2. This is likely because h_{ind} tends to co-vary in the west and southwest Pacific, as the spatial pattern of ENSO-related windstress remains at first order similar among ENSO events (the present study focusses on typical ENSO events and neglect 2nd order spatial diversity). Concerning R_o, ε_o and F_{2_o} spatial patterns, they can be explained by the following relationships: $R_o \approx \varepsilon_o \approx -KF_1$ and $F_{2\_o} \approx F_2 + K^2F_1$ (as $\varepsilon \approx 0$ and $R \approx 0$).

3.2 Objectively finding the optimal region : West and South-West (h_{ind_w+sw})

The optimal region for $h_{ind}(x,y,t)$ will be the one optimizing the skill of the RO tendency equation for $\begin{pmatrix} T_E \\ h_{ind} \end{pmatrix}$:

$$\frac{d\begin{pmatrix} T_E \\ h_{ind} \end{pmatrix}}{dt} = \begin{pmatrix} R & F_1 \\ -F_2 & -\varepsilon \end{pmatrix}\begin{pmatrix} T_E \\ h_{ind} \end{pmatrix} \qquad (9)$$

Its skill is $r_{T_e,h\_ind} = ((r_{T_e}^2 + r_{h\_ind}^2)/2)^{1/2}$ (Fig. 1i). The best averaging region should be the western equatorial Pacific (~5°N-5°S), but also the southwest (~5°S-15°S). This agrees with Izumo et al. (2018a) which suggest to use a western Pacific OHC index extended to the southwestern Pacific, because of ENSO meridional asymmetries (see also Santoso et al. 2017; Ramesh and Murtugudde 2013).

The skill should be even better if we average spatially h_{ind}(x,y,t) to reduce noise. To choose objectively the optimal rectangular averaging region, we have averaged h_{ind}(x,y,t) from the usual fixed 120°E western end (western Pacific being anyway essential; Fig. 1i) to a varying eastern end, for various latitudinal bands (Fig. 2, Suppl. Fig. S3). For the classical 5°N-5°S band, the best skill is found for an eastern end of the box varying in between ~160°W and ~120°W. The 5°N-15°S band gives the best skill, for an eastern boundary around ~155°W, consistent with Fig. 1i. So the best rectangular box is like the WWV_{west} box (5°N-5°S, 120°E-155°W) with its southern boundary extended to 15°S, i.e. h_{ind_w+sw}. Now onwards this h_{ind_w+sw} will be our default best recharge index. Note that we chose a rectangle for simplicity.

Using this index, normalized, we obtain: $F_1=0.14\pm0.03$, $R=0.00\pm0.03$, $F_2=0.14\pm0.03$, $\varepsilon=0.00\pm0.03$ (unit: month^{-1}). R and ε are still negligible. This reduces the parameter space and the RO equations system has the form of an undamped harmonic oscillator excited by noise (Burgers et al. 2005), with $d^2X(t)/dt^2 \approx -F_1F_2\,X(t)$, $X(t)$ being T_E or h_{ind}, and angular frequency being the Wyrtki index $W=(F_1F_2)^{1/2}$ (i.e. eigenperiod of ~3.7 year).

Note that, if we had used the full h_{w+sw} instead of h_{ind_w+sw}, then we would have for the equation $dh_{w+sw}/dt = -\varepsilon_o h_{w+sw} - F_{2\_o}T_E$ a damping ε_o which would be significantly positive, and thus not negligible (Fig. 1e). Indeed, as $\varepsilon_o = \varepsilon - KF_1$, with $K<0$ and $F_1>0$, i.e. $KF_1<0$, in this region, ε_o is significantly positive, even if the actual damping ε is weak. This is consistent with Jin (1997a). He shows that the damping term decreases if h_{w+e} is used instead of h_w, as h_{w+e} is not correlated to T_E , while h_w is, in Jin (1997a) simplified model. Similarly, for the dT_E/dt equation, as $R_o = R - KF_1$, R_o is significantly positive (Fig. 1a), even if the actual net feedback R is weak. So the "damping" term (ε_o) and the "positive feedback" (R_o) would be artificially large. This further confirms that we should use h_{ind} rather than the full h polluted by the fast mode that biases the RO model.

3.3 Discussion on the mechanisms behind T_E and h_{ind} tendency equations

Here we first discuss the physical mechanisms behind the term $F_1h_{ind\_w+sw}$. Different mechanisms have been suggested to explain why a deepening of the thermocline depth related to a recharge favors positive T_E. Originally the thermocline feedback was invoked, firstly in the eastern Pacific (Wyrtki 1985, Jin 1997ab), and later in the central Pacific since coupling with convection is larger there (Clarke et al. 2007). Previous studies have suggested that the western-central Pacific recharge can slowly favor a background deepening of the central-eastern thermocline depth independent of the zonal tilt mode, because of the tilt mode balance: $h_e \approx \beta_T T_E + h_w$ (using Jin et al. 2020 notations). This would favor positive T_E through the thermocline feedback. The deeper thermocline in the southwest and equatorial Pacific can also favor warmer transport-weighted temperatures of the meridional pycnocline convergence T_{conv} (especially because pycnocline convergence is larger in the southwest than in the northwest) and/or of the equatorial undercurrent (EUC) T_{EUC} (e.g. Izumo 2005, Ballester et al. 2015, 2016ab), i.e. of the lower branches of the shallow meridional overturning cells (STCs). This can also favor warmer upwelled waters and thus warmer SST in the central-eastern equatorial Pacific. Concerning the southwest Pacific recharge, we can hypothesize two additional roles it can play. 1) The anomalous windstress curl there forces off-equatorial downwelling (in the La Niña case) Rossby waves that propagates to the Pacific equatorial band as Kelvin waves, through western boundary coastal wave guide and equatorial wave guide, and progressively favors a recharge of OHC there, all along the equatorial Pacific. 2) Once recharged, the southwest Pacific recharge could play a role in favoring downwelling equatorial Kelvin wave when winds are set back to neutral, through the same wave pathway. These two can both influence T_E through the thermocline feedback and STCs transport-weighted temperatures. Whatever the relative contributions of these various mechanisms, their influence on T_E can be formalized as a term linearly proportional to h_{w+sw} at first order: $F_1h_{ind\_w+sw}$.

The proposed mechanisms behind h_{ind_w+sw} recharge process, the term $-F_2T_E$, are the following. E.g. during a La Niña, easterlies favor a slow recharge in the southwestern, western

and equatorial Pacific through: 1) downwelling equatorial Rossby waves to the west (Wyrtki 1985, Jin 1997ab), and off-equatorial ones in the southwest (Suppl. Fig. S2); 2) upwelling equatorial Kelvin waves to the east forcing coastal Kelvin waves propagating poleward along the eastern boundary and thus a leakage of negative OHC anomalies towards the poles along the eastern boundary (Wyrtki 1985, Izumo et al. 2018a). The recharge has also been suggested to be through Sverdrup transport towards the equator (Jin 1997a,b) but this is now debated (Clarke 2010; Zhu et al. 2018; Izumo et al. 2018a). Whatever the mechanisms, they are all formally well represented by the term $-F_2T_E$.

4 Conclusion

4.1 Summary

Here we have defined a simple Pacific OHC recharge index *independent* of the fast mode, by regressing out T_E-related variability: h_{ind}. It unambiguously represents the slow recharge mode, conversely to classical OHC indices. It also allows us to have more physical RO equations. The damping term becomes notably negligible for the recharge mode. We have objectively searched for the optimal OHC averaging region to have the most realistic RO T_E and h_{ind} tendency equations. The optimal index is h_{ind_w+sw} averaged over the classical WWV_{west} region (5°N-5°S, 120°E-155°W) extended to the southwest until 15°S (5°N-15°S, 120°E-155°W). The southwest recharge is caused by ENSO meridionally-asymmetric Ekman pumping.

4.2 Implications for ENSO seasonal forecasts: *interest of using h_{ind} for ENSO operational forecasts*

For ENSO operational forecast diagnostics, the pair of coordinates (T_E,h_{ind_w+sw}) is more relevant to describe the system trajectory than the (T_E,h_{w+sw}) pair (Fig. 3). If the latter is used, a situation with anomalous h_{w+sw} is ambiguous: it does not necessarily correspond to a recharge/discharge state, as the fast tilt mode signal could blur a weaker long-term build-up of heat content. Independent h_{ind_w+sw} better represents actual precursory OHC preconditioning anomalies. It is geometrically simply a linear transform of coordinates from the (T_E, h_{w+sw}) space to the (T_E, h_{ind_w+sw}) orthogonal coordinates space. The observed trajectory in the later space is more circular, and more relevant for operational forecast diagnostics: $h_{ind\_w+sw}>0$ unambiguously corresponds to a recharged preconditioning state, clearly separated from the simultaneous ENSO T_E conditions (e.g. ENSO biennal tendency), while $h_{w+sw}>0$ is not sufficient to conclude.

In practice, obtaining h_{ind_w+sw} is straightforward: 1) average over (5°N-15°S, 120°E-155°W) the satellite SLA (using $h(x,y,t) \sim SLA(x,y,t)$, detrended, smoothed, with seasonal cycle removed, cf. section 2), 2) remove its dependent part KT_E, with regression coefficient $K = -2.2$ cm/ºC: $h_{ind\_w+sw} = h_{w+sw} - KT_E$, T_E being Niño3.4 relative SST anomaly (smoothed) in ºC.

4.3 Discussion

Here we have neglected possible seasonal cycles of parameters and asymmetries/non-linearities for the sake of simplicity. Knowing ENSO seasonal phase-locking, taking into account such seasonal cycles could be one next step. We could include asymmetrical/non-linear terms, e.g. quadratic terms (non-linear response of convection to T_E; e.g. Jin et al. 2020) and a multiplicative noise (e.g. Jin et al. 2007, Graham et al. 2015, their equation (23)). To have a simple h_{ind} definition, we have also neglected a weak non-linearity in the fast response of h to T_E: a slightly larger negative slope of the $h_{w+sw}(T_E)$ relationship for negative h_{w+sw} (Fig. 3a). This weak non-linearity is likely due to τ_x anomalies longitudinal position, further to the east during El Niño than during La Niña, favoring a larger rapid discharge of the western equatorial Pacific. This non-linearity would lead to a quadratic term in the dh_{ind}/dt equation.

Some studies, using usual h indices, have put in question the RO and suggested that the delayed oscillator (DO, Suarez and Schopf 1988, Battisti and Hirst 1989) is more realistic (e.g. Linz et al. 2014, Graham et al. 2015). One reason for this "RO vs DO" debate could be the misleading character of usual h indices because of their dependent component. Testing each ENSO oscillator, using h_{ind_w+sw} instead, would be interesting to see whether theories, climate models and observations would then better agree.

Acknowledgements. We would like to thank Dr. Matthieu Lengaigne, Dr. Jérôme Vialard, and Pr. Fei-Fei Jin for some great discussions on this work. T.I. would like to thank the UPF for hosting M.C. because of COVID-related closed Australian borders; this latter fact was paradoxically essential for allowing us to make this work mature.

Open Research (Data Availability Statement). All data used is open data: OISSTv2 (https://psl.noaa.gov/data/gridded/data.noaa.oisst.v2.html), CMAP1 (https://psl.noaa.gov/data/gridded/data.cmap.html) ERA-I (https://www.ecmwf.int/en/forecasts/datasets/reanalysis-datasets/era-interim), CSIRO SLA (http://www.cmar.csiro.au/sealevel/sl_data_cmar.html). We acknowledge the use of NOAA pyferret open source software for analyses and figures.

References

Alory, G., & Delcroix, T. (2002). Interannual sea level changes and associated mass transports in the tropical Pacific from TOPEX/Poseidon data and linear model results (1964–1999). *Journal of Geophysical Research: Oceans*, *107*(C10), 17-1.

Ballester, J., Bordoni, S., Petrova, D., & Rodó, X. (2015). On the dynamical mechanisms explaining the western Pacific subsurface temperature buildup leading to ENSO events. *Geophysical Research Letters*, *42*(8), 2961-2967.

Ballester, J., Petrova, D., Bordoni, S., Cash, B., García-Díez, M., & Rodó, X. (2016a). Sensitivity of El Niño intensity and timing to preceding subsurface heat magnitude. *Scientific reports*, *6*(1), 1-9.

Ballester, J., Bordoni, S., Petrova, D., & Rodó, X. (2016b). Heat advection processes leading to El Niño events as depicted by an ensemble of ocean assimilation products. *Journal of Geophysical Research: Oceans*, *121*(6), 3710-3729.

Barnston, A. G., Tippett, M. K., L'Heureux, M. L., Li, S., & DeWitt, D. G. (2012). Skill of real-time seasonal ENSO model predictions during 2002–11: Is our capability increasing?. *Bulletin of the American Meteorological Society*, *93*(5), 631-651.

Barnston, A. G., Tippett, M. K., Ranganathan, M., & L'Heureux, M. L. (2019). Deterministic skill of ENSO predictions from the North American Multimodel Ensemble. *Climate Dynamics*, *53*(12), 7215-7234.

Battisti, D. S., & Hirst, A. C. (1989). Interannual variability in a tropical atmosphere–ocean model: Influence of the basic state, ocean geometry and nonlinearity. *Journal of Atmospheric Sciences*, *46*(12), 1687-1712.

Boschat, G., Terray, P., & Masson, S. (2013). Extratropical forcing of ENSO. *Geophysical Research Letters*, *40*(8), 1605-1611.

Bretherton, C. S., Widmann, M., Dymnikov, V. P., Wallace, J. M., & Bladé, I. (1999). The effective number of spatial degrees of freedom of a time-varying field. *Journal of climate*, *12*(7), 1990-2009.

Burgers, G., F.-F. Jin, and G. J. van Oldenborgh (2005), The simplest ENSO recharge oscillator, Geophys. Res. Lett., 32, L13706, doi:10.1029/2005GL022951.

Capotondi, A., Wittenberg, A. T., Newman, M., Di Lorenzo, E., Yu, J. Y., Braconnot, P., ... & Yeh, S. W. (2015). Understanding ENSO diversity. *Bulletin of the American Meteorological Society*, *96*(6), 921-938.

Cibot, C., Maisonnave, E., Terray, L., & Dewitte, B. (2005). Mechanisms of tropical Pacific interannual-to-decadal variability in the ARPEGE/ORCA global coupled model. *Climate dynamics*, *24*(7), 823-842.

Clarke, A. J., Van Gorder, S., & Colantuono, G. (2007). Wind stress curl and ENSO discharge/recharge in the equatorial Pacific. *Journal of Physical Oceanography*, *37*(4), 1077-1091.

Clarke, A. J. (2008). *An introduction to the dynamics of El Niño and the Southern Oscillation*. Elsevier.

Clarke, A. J. (2010). Analytical theory for the quasi-steady and low-frequency equatorial ocean response to wind forcing: The "tilt" and "warm water volume" modes. *Journal of physical oceanography*, *40*(1), 121-137.

Dee, D. P., Uppala, S. M., Simmons, A. J., Berrisford, P., Poli, P., Kobayashi, S., & Bechtold, P. (2011). The ERA-Interim reanalysis: Configuration and performance of the data

assimilation system. *Quarterly Journal of the Royal Meteorological Society*, *137*(656), 553–597.

Fedorov, A. V. (2010). Ocean response to wind variations, warm water volume, and simple models of ENSO in the low-frequency approximation. *Journal of climate*, *23*(14), 3855-3873.

Gadgil, S., Joseph, P. V., & Joshi, N. V. (1984). Ocean–atmosphere coupling over monsoon regions. *Nature*, *312*(5990), 141-143.

Graham, F. S., Brown, J. N., Wittenberg, A. T., & Holbrook, N. J. (2015). Reassessing conceptual models of ENSO. *Journal of Climate*, *28*(23), 9121-9142.

Izumo, T. (2005). The equatorial undercurrent, meridional overturning circulation, and their roles in mass and heat exchanges during El Niño events in the tropical Pacific Ocean. *Ocean Dynamics*, *55*(2), 110-123.

Izumo, T., Vialard, J., Dayan, H., Lengaigne, M., & Suresh, I. (2016). A simple estimation of equatorial Pacific response from windstress to untangle Indian Ocean Dipole and Basin influences on El Niño. *Climate dynamics*, *46*(7-8), 2247-2268.

Izumo, T., Lengaigne, M., Vialard, J., Suresh, I., & Planton, Y. (2018a). On the physical interpretation of the lead relation between Warm Water Volume and the El Niño Southern Oscillation. *Climate Dynamics*, *52*(5), 2923-2942.

Izumo, T., Khodri, M., Lengaigne, M., & Suresh, I. (2018b). A subsurface Indian Ocean dipole response to tropical volcanic eruptions. *Geophysical Research Letters*, *45*(17), 9150-9159.

Izumo, T., Vialard, J., Lengaigne, M., & Suresh, I. (2020). Relevance of relative sea surface temperature for tropical rainfall interannual variability. *Geophysical Research Letters*, *47*(3), e2019GL086182.

Jin, F. F. (1997a). An equatorial ocean recharge paradigm for ENSO. Part I: Conceptual model. *Journal of the atmospheric sciences*, *54*(7), 811-829.

Jin, F. F. (1997b). An equatorial ocean recharge paradigm for ENSO. Part II: A stripped-down coupled model. *Journal of Atmospheric Sciences*, *54*(7), 830-847.

Jin, F.-F., Lin, L., Timmermann, A., & Zhao, J. (2007). Ensemble- mean dynamics of the ENSO recharge oscillator under state- dependent stochastic forcing. *Geophysical Research Letters*, *34*(3), L03807. https://doi.org/10.1029/2006GL027372

Jin, F. F., Chen, H. C., Zhao, S., Hayashi, M., Karamperidou, C., Stuecker, M. F., ... & Geng, L. (2020). Simple ENSO models. *El Niño Southern Oscillation in a Changing Climate*, 119-151.

Johnson, N. C., & Xie, S.-P. (2010). Changes in the sea surface temperature threshold for tropical convection. *Nature Geoscience*, *3*(12), 842–845.

Johnson, N. C., & Kosaka, Y. (2016). The impact of eastern equatorial Pacific convection on the diversity of boreal winter El Niño teleconnection patterns. *Climate Dynamics*, *47*(12), 3737-3765.

Khodri, M., Izumo, T., Vialard, J., Janicot, S., Cassou, C., Lengaigne, M., ... & McPhaden, M. J. (2017). Tropical explosive volcanic eruptions can trigger El Niño by cooling tropical Africa. *Nature communications*, *8*(1), 1-13.

Lai AWC, Herzog M, Graf HF (2015) Two key parameters for the El Niño continuum: zonal wind anomalies and Western Pacific sub- surface potential temperature. Clim Dyn 45(11–12):3461–3480. https://doi.org/10.1007/s00382-015-2550-0

Lengaigne M, Boulanger J-P, Menkes C, Spencer H (2006) Influence of the seasonal cycle on the termination of El Niño events in a coupled general circulation model. J Clim 19(9):1850–1868. https ://doi.org/10.1175/JCLI3706.1

Linz M, Tziperman E, MacMartin DG (2014) Process-based analysis of climate model ENSO simulations: intermodel consistency and compensating errors. J Geophys Res 119:7396–7409. https://doi. org/10.1002/2013JD021415

Masuda, S., Awaji, T., Toyoda, T., Shikama, Y., & Ishikawa, Y. (2009). Temporal evolution of the equatorial thermocline associated with the 1991–2006 ENSO. *Journal of Geophysical Research: Oceans*, *114*(C3).

Meinen CS, McPhaden MJ (2000) Observations of warm water volume changes in the equatorial Pacific and their relationship to El Niño and La Niña. J Clim 13:3551–3559

Neelin, J. D., Battisti, D. S., Hirst, A. C., Jin, F. F., Wakata, Y., Yamagata, T., & Zebiak, S. E. (1998). ENSO theory. *Journal of Geophysical Research: Oceans*, *103*(C7), 14261-14290.

Neske S, McGregor S (2018) Understanding the warm water volume precursor of ENSO events and its interdecadal variation. Geophys Res Lett 45:1577–1585. https://doi.org/10.1002/2017GL076439

Okumura, Y. M. (2019). ENSO diversity from an atmospheric perspective. *Current Climate Change Reports*, *5*(3), 245-257.

Petrova, D., Koopman, S. J., Ballester, J., & Rodó, X. (2017). Improving the long-lead predictability of El Niño using a novel forecasting scheme based on a dynamic components model. *Climate Dynamics*, *48*(3-4), 1249-1276.

Ramesh N, Murtugudde R (2013) All flavours of El Niño have similar early subsurface origins. Nat Clim Change 3(1):42–46. https://doi. org/10.1038/nclimate1600

Reynolds, R.W., N.A. Rayner, T.M. Smith, D.C. Stokes, and W. Wang, 2002: An improved in situ and satellite SST analysis for climate. J. Climate, 15, 1609-1625.

Santoso, A., Mcphaden, M. J., & Cai, W. (2017). The defining characteristics of ENSO extremes and the strong 2015/2016 El Niño. Reviews of Geophysics, 55, 1079–1129.

Suarez MJ, Schopf PS (1988) A delayed action oscillator for ENSO. J Atmos Sci 45:3283–3287

Takahashi K, Montecinos A, Goubanova K, Dewitte B (2011) ENSO regimes: reinterpreting the canonical and Modoki El Niño. Geo- phys Res Lett 38:1–5. https://doi.org/10.1029/2011GL047364

Thual S,.Dewitte B, Ayoub N, Thual O (2013) An asymptotic expansion for the recharge–discharge model of ENSO. J Phys Oceanogr 43:1407–1416. https://doi.org/10.1175/JPO-D-12-0161.1

Timmermann, Axel, et al. "El Niño–southern oscillation complexity." *Nature* 559.7715 (2018): 535-545.

Van Oldenborgh, G. J., Hendon, H., Stockdale, T., L'Heureux, M., De Perez, E. C., Singh, R., & Van Aalst, M. (2021). Defining El Niño indices in a warming climate. *Environmental Research Letters*, *16*(4), 044003.

Wang, C., & Picaut, J. (2004). Understanding ENSO physics—A review. *Earth's Climate: The Ocean–Atmosphere Interaction, Geophys. Monogr*, *147*, 21-48.

Williams, I. N., & Patricola, C. M. (2018). Diversity of ENSO events unified by convective threshold sea surface temperature: A nonlinear ENSO index. *Geophysical Research Letters*, *45*(17), 9236-9244.

Wyrtki K (1985) Water displacements in the Pacific and the genesis of El Niño cycles. J Geophys Res 90:7129–7132.

Xie, P., & Arkin, P. A. (1997). Global precipitation: A 17-year monthly analysis based on gauge observations, satellite estimates, and numerical model outputs. *Bulletin of the American Meteorological Society*, *78*(11), 2539–2558.

Yokoi, T., Tozuka, T., & Yamagata, T. (2008). Seasonal variation of the Seychelles Dome. *Journal of Climate*, *21*(15), 3740-3754.

Zhu, X., Greatbatch, R. J., & Claus, M. (2017). Interannual variability of tropical Pacific sea level from 1993 to 2014. *Journal of Geophysical Research: Oceans*, *122*(1), 602-616.

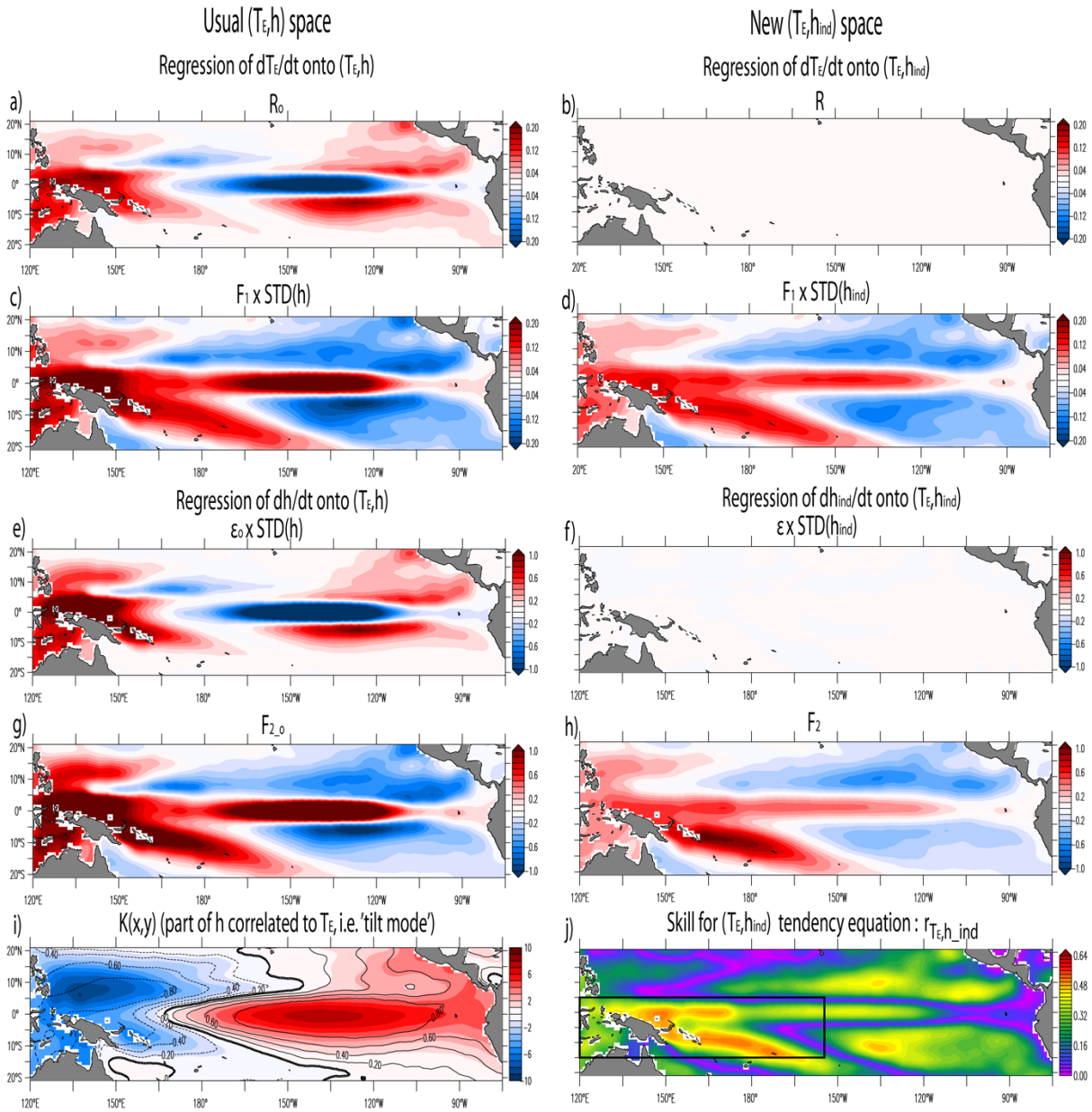

Fig. 1. Searching for the optimal recharge index h_{ind}, representing the actual slow recharge mode independent of the fast mode in RO equations. Panels **a** and **c** show respectively the coefficients $R_o(x,y)$ and $F_1(x,y)$ for the multivariate regression of $dT_E/dt(t)$ onto $T_E(t)$ and $h(x,y,t)$ (equation 4). To be able to compare their respective contributions to the regression, $F_1(x,y)$ is multiplied by STD(h(x,y,t)) (T_E is already standardized). Panels **b** and **d** are as a and c, but for $R(x,y)$ and $F_1(x,y)$ for the multivariate regression of $dT_E/dt(t)$ onto $T_E(t)$ and $h_{ind}(x,y,t)$ (equation 7). Panels **e**,**f**,**g**,**h** are as a,b,c,d, but for the regression of $dh(x,y,t)/dt$ or $dh_{ind}(x,y,t)/dt$: left panels **e** and **g** correspond to equation (5) for usual (T_E,h), right panels **f** and **h** to equation (8) for (T_E,h_{ind}) instead. Panel **i** shows the component of $h(x,y,t)$ dependent of $T_E(t)$, i.e. the coefficient $K(x,y)$ of the regression of $h(x,y,t)$ onto $T_E(t)$ in color shading (equation 6), which represents the fast tilt mode (correlation in black contours). Panel **j** shows the correlation skill for the tendency equation of the vector (Te,h_{ind}) (equation 9): $r_{Te,h\_ind} = ((r_{Te}^2 + r_{h\_ind}^2)/2)^{1/2}$, where r_{Te} and r_{h_ind} are the correlations for dT_E/dt and dh_{ind}/dt equations respectively (shown in Suppl. Fig. S1). The black box overlaid represents the West+SouthWest (*w+sw*) rectangular box finally chosen to average h_{ind}. See text for details.

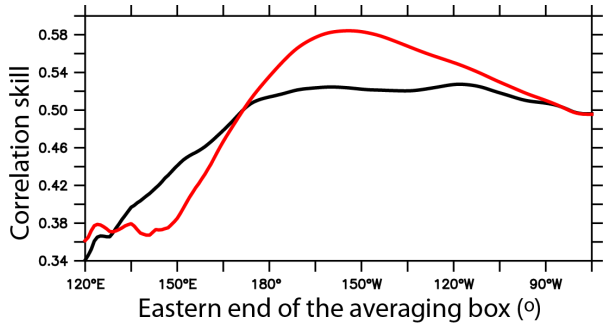

Fig. 2. Finding the best averaging box for h_{ind} to optimize both T_E and h_{ind} tendency equations of RO. Skill $r_{Te,h\_ind}(x) = ((r_{Te}^2 + r_{h\_ind}^2)/2)^{1/2}$, for h_{ind} averaged over a box with its western boundary fixed to 120°E and its eastern boundary given by the x-axis, with box latitudinal width fixed to 5°N-5°S (black) or 5°N-15°S (red; Suppl. Fig. S3 tests other widths). The optimal rectangular box is from 120°E to ~155°W (indicated as a dashed vertical line), 5°N-15°S width. This defines the new index: $h_{ind\ w+sw}$**.**

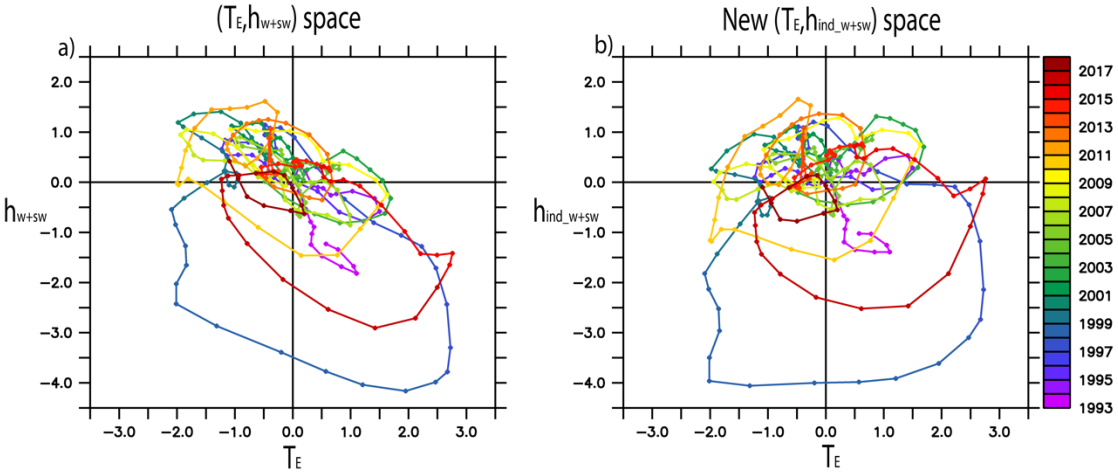

Fig. 3. Observed trajectory of the RO in the (T_E,h_{w+sw}) and (T_E,h_{ind_w+sw}) spaces. a) trajectory of the system for the pair of coordinates (T_E,h_{w+sw}), each month being a point, with year indicated in color. b) same for orthogonal coordinates (T_E,h_{ind_w+sw}). h_{w+sw} and h_{ind_w+sw} are averaged over the western and southwestern Pacific (box shown in Fig. 1j). *Te*, h_{w+sw} and $h_{ind\ w+sw}$ are normalised.

Geophysical Research Letters

Supporting Information for

Improving the oceanic metric of the El Niño recharge oscillator model

Takeshi Izumo[1,2] and Maxime Colin[3,4,5]

[1] Institut de Recherche pour le Développement (IRD), EIO laboratory, Université de la Polynésie Française (UPF), Tahiti, French Polynesia

[2] formerly at IRD, Sorbonne Université - CNRS-IRD-MNHN, LOCEAN Laboratory, IPSL, Paris, France

[3]formerly at Climate Change Research Centre, University of New South Wales, Sydney, New South Wales, Australia

[4]Leibniz Centre for Tropical Marine Research, Bremen, Germany

[5]formerly at Laboratoire GEPASUD, University of French Polynesia, Tahiti, French Polynesia

Contents of this file

Introduction

The supplementary information contains 3 supplementary figures:

- Suppl. Fig. S1. Respective contributions of the r_{Te} skill and r_{h_ind} skill to the r_{Te,h_ind} skill.
- Suppl. Fig. S2. ENSO asymmetrical Ekman pumping.
- Suppl. Fig. S3. Testing other possible latitudinal bands for h_{ind} averaging box (Fig. 2).

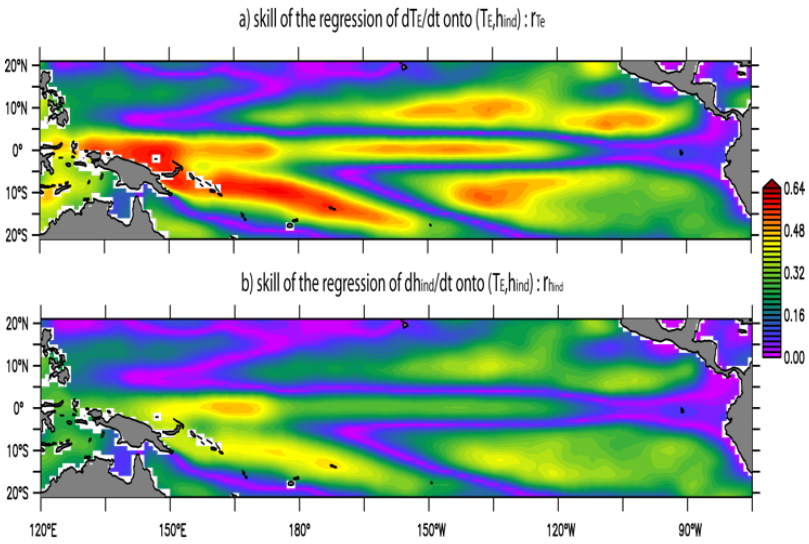

Suppl. Fig. S1. Respective contributions of the r_{Te} skill and r_{h_ind} skill to the r_{Te,h_ind} skill. a) correlation skill r_{Te} for the regression of dT_E/dt onto $(Te(t),h_{ind}(x,y,t))$ (corresponding to equation 7 and Fig. 1b,d). b) same but for r_{h_ind} (corresponding to equation 8 and Fig. 1f,h). They both contribute to the skill r_{Te,h_ind} shown in Fig. 1j for the tendency equation of the vector (Te,h_{ind}), since $r_{Te,h\_ind} = ((r_{Te}^2 + r_{h\_ind}^2)/2)^{1/2}$. Note that r_{Te} tends to have a similar spatial pattern to r_{h_ind}, but of stronger amplitude. The similarity of the spatial pattern, notably with the strongest skill in the west and southwest Pacific, is likely because h_{ind} tends to vary in phase in the west and southwest. r_{Te} tends to be of larger amplitude than r_{h_ind}, partly because $dT_E(t)/dt$ is less noisy, T_E being a box average, than $dh_{ind}(x,y,t)/dt$, which is for each (x,y) point. The pair $(Te(t),h_{ind}(x,y,t))$ can thus more easily explain $dT_E(t)/dt$ variance than dh_{ind}/dt variance.

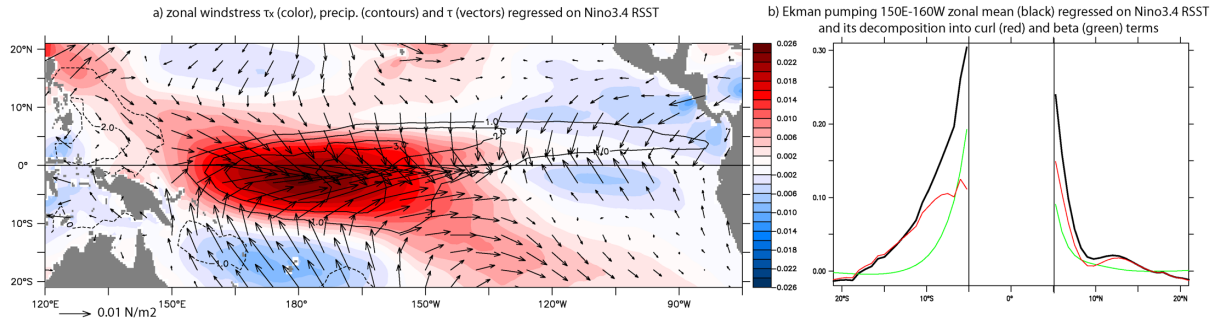

Suppl. Fig. S2. ENSO asymmetrical Ekman pumping. a) Zonal windstress τ_x (color, $N.m^{-2}$), precipitation (contours, $mm.day^{-1}$) and windstress τ (vectors) regressed on T_E. **b)** Regression of the 150°E-140°W zonal mean of Ekman pumping (black, 10^{-5}m/s) on T_E, and Ekman pumping decomposition into its windstress curl (red) and beta τ_x (green) terms, only defined out of the 5°N-5°S equatorial band (shown by vertical lines). In the southern hemisphere, the decomposition shows that south of ~7°S, the windstress curl term is the main contributor to Ekman pumping, while north of ~7°S, the beta term is also important.

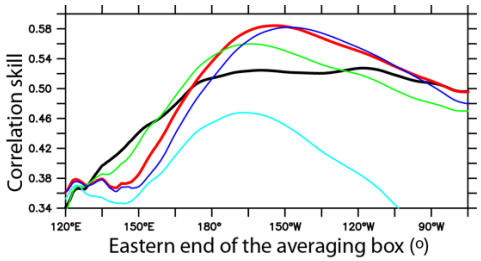

Suppl. Fig. S3. Testing other possible latitudinal bands for the h_{ind} averaging box. As Fig. 2, still with 5°N-5°S in black and 5°N-15°S in red, but testing also 10°N-10°S in light blue, 5°N-10°S in green and 5°N-20°S in dark blue.